(27) Granger, A. T.; Wang, B.; Krause, S.; Fetters, L. J. *Adv. Chem. Ser.* **1986**, *No. 211*, 127.
(28) Krause, S.; Lu, Z.-H.; Iskandar, M. *Macromolecules* **1982**, *15*, 1076.
(29) Krause, S.; Iskandar, M. *Adv. Chem. Ser.* **1979**, *No. 176*, 205.
(30) Hashimoto, T.; Tsukahara, T.; Tachi, K.; Kawai, H. *Macromolecules* **1983**, *16*, 648.
(31) Guar, U.; Wunderlich, B. *Macromolecules* **1980**, *13*, 1618.
(32) Fox, T. G. *Bull. Am. Phys. Soc.* **1956**, *2*, 123.
(33) MacKnight, W. J.; Karasz, F. E.; Fried, J. R. In *Polymer Blends*; Paul, D. R., Newman, S., Eds.; Academic: New York, 1978; Vol. 1, Chapter 5.
(34) Keskkula, H.; Paul, D. R.; Young, P.; Stein, R. S. *J. Appl. Polym. Sci.* **1987**, *34*, 1861.
(35) Fried, J. R.; Lorenz, T.; Ramdas, A. *Polym. Eng. Sci.* **1985**, *25*, 1048.
(36) Fried, J. R.; Hanna, G. A. *Polym. Eng. Sci.* **1982**, *22*, 705.
(37) Shultz, A. R.; Beach, B. M. *Macromolecules* **1974**, *7*, 902.
(38) Fernandes, A. C. Doctoral Dissertation, University of Texas, 1986.
(39) Bohn, L. *Adv. Chem. Ser.* **1975**, *No. 142*, 66. Kraus, G.; Fodor, L. M.; Rollman, K. W. *Polym. Prepr. (Am. Chem. Soc., Div. Polym. Chem.)* **1978**, *19*, 68. Krause, S.; Wang, B. *J. Polym. Sci., Polym. Lett. Ed.* **1986**, *24*, 35.
(40) Bates, F. E.; Cohen, R. E.; Argon, A. S. *Macromolecules* **1983**, *16*, 1108.
(41) Nielsen, L. *Mechanical Properties of Polymers and Composites*; Marcel Dekker: New York, 1974; Vol. 2.
(42) Kerner, E. H. *Proc. Phys. Soc.* **1956**, *69B*, 808.
(43) Faucher, J. A. *J. Polym. Sci., Polym. Phys. Ed.* **1974**, *12*, 2153.
(44) Aggarwal, S. L. *Polymer* **1976**, *17*, 938.
(45) Kleiner, L. W.; Karasz, F. E.; MacKnight, W. J. *Polym. Eng. Sci.* **1979**, *19*, 519.
(46) Kraus, G.; Rollman, K. W.; Gardner, J. O. *J. Polym. Sci., Polym. Phys. Ed.* **1972**, *10*, 2061.
(47) Odell, J. A.; Keller, A. *Polym. Eng. Sci.* **1977**, *17*, 544.
(48) Meier, D. J. In *Block and Graft Copolymers*; Burke, J. J., Weiss, V., Eds.; Syracuse University Press: New York, 1973; Chapter 6.
(49) Kato, K. *J. Polym. Sci., Part B* **1966**, *4*, 35; *Polym. Eng. Sci.* **1967**, *7*, 38.
(50) Niinomi, M.; Katsuta, T.; Kotani, T. *J. Appl. Polym. Sci.* **1975**, *19*, 2919.
(51) Meier, D. J. *Polym. Prepr. (Am. Chem. Soc., Div. Polym. Chem.)* **1977**, *18*, 340.
(52) Noolandi, J.; Hong, K. M. *Polym. Bull.* **1982**, *7*, 561; *Macromolecules* **1983**, *16*, 1083; *Ber. Bunsen-Ges. Phys. Chem.* **1985**, *89*, 1147.
(53) Xie, H.; Liu, Y.; Jiang, M.; Yu, T. *Polymer* **1986**, *27*, 1928.
(54) Alward, D. B.; Kinning, D. J.; Handlin, D. L.; Thomas, E. L.; Fetters, L. J. *Macromolecules* **1986**, *19*, 215; **1986**, *19*, 1288; **1986**, *19*, 2197.

Solute Diffusion in Polymers. 2. Fourier Estimation of Capillary Column Inverse Gas Chromatography Data

Craig A. Pawlisch,† John R. Bric,‡ and Robert L. Laurence*

Department of Chemical Engineering, University of Massachusetts, Amherst, Massachusetts 01003. *Received October 15, 1987; Revised Manuscript Received December 17, 1987*

ABSTRACT: Moment analysis of capillary column inverse gas chromatography (IGC) data provides accurate measurement of polymer–solute diffusion coefficients. The technique is ideal for studying interactions of volatile materials with molten or rubbery polymers, at conditions approaching infinite dilution of the volatile component. The analysis presented by Pawlisch et al.,[1] however, can provide flawed results if the geometry of the column coating is not uniform or if the polymer/solute system exhibits elution curves with significant skewing. In this paper, we present two improvements that overcome these limitations: (1) a model that accounts for a nonuniform polymer film and (2) a method for parameter estimation in the Fourier domain. The usefulness of the improvements is demonstrated by measuring the diffusivity and activity of benzene, toluene, and ethylbenzene in polystyrene, between 110 and 140 °C, the system investigated in part 1, and of methanol, methyl acetate, and methyl methacrylate in poly(methyl methacrylate) at temperatures above the glass transition temperature. In addition, the IGC technique is demonstrated to be applicable at temperatures below the glass transition temperature, as successful sub-T_g measurements were made for methanol in poly(methyl methacrylate). Finally, criteria are presented for the experimental modifications necessary to reduce the skewing of elution curves, which can reduce the reliability of results.

Introduction

Inverse gas chromatography (IGC) is now well established as a means of studying interactions between polymers and volatile solutes. In a typical application, the polymer is used as the stationary phase of a chromatographic column, while a pulse of the volatile solute is vaporized and injected into a carrier gas that flows through the column. The retention time and the elution profile of the solute pulse, affected by interactions between the solute and the stationary phase, can be used to study those interactions. Because the volume of injected solute (sometimes referred to as a probe) is small (0.2 μL of liquid), interactions between the probe and the stationary phase generally occur at solute concentrations approaching infinite dilution. Depending upon the physical state of the polymer and the nature of the probe, a wide variety of physical and/or chemical properties can be measured. Reported applications of the technique include measurements of thermodynamic properties of solutions, surface sorption characteristics, phase-transition temperatures, and degree of crystallinity of the polymeric phase. These applications have been reviewed in detail by several authors.[2-5]

IGC has also been proposed as a means of studying diffusion of solutes within a polymeric material. It has long been recognized that transport limitations in the stationary phase can produce significant broadening and distortion of a chromatographic peak. A number of researchers have attempted to exploit this phenomenon as a means of measuring the diffusion coefficient of the probe substance in the stationary phase.[6-11] In all of these studies, packed

† Current address: Research Laboratories, Union Camp Corp., Princeton, NJ.
‡ Polymer Science and Engineering Department, University of Massachusetts.

0024-9297/88/2221-1685$01.50/0

column chromatography was employed, and diffusion coefficient estimates were extracted from elution curve data via application of the van Deemter equation. None of these efforts provided a convincing demonstration that the method can be used to obtain accurate, reliable estimates of the diffusion coefficient; difficulties inherent in the use of a packed column make it nearly impossible to relate the shape of the elution curve to the diffusion coefficient. The major limitation is the irregular distribution of the stationary phase within the column, which prohibits application of realistic models for stationary phase transport processes. Two recent, carefully done studies[12,13] show improvements in the use of packed columns, but both indicate the inappropriateness of packed columns for diffusion studies, given that calibration with a primary technique is required.

In the first paper[1] of this series, we have shown that by the use of a uniformly coated capillary column, this limitation can be eliminated. Reliable estimates of the solute diffusion coefficient were obtained from the degree of peak broadening, by using a mathematical model that assumes a uniform, annular coating of polymer. A moment analysis of the elution curve was used to obtain the parameter estimates. The effectiveness of the technique was demonstrated in a study of benzene, toluene, and ethylbenzene in polystyrene.

In this paper, we expand upon the model introduced in part 1 to incorporate the effect of small deviations in the uniformity of the polymer coating. The model used in part 1[1] assumes that the polymer is deposited in the column as an annular film of uniform thickness. Although the coating procedure outlined in part 1 does produce annular coatings with a uniform axial distribution of polymer, the coatings may exhibit a small eccentricity when viewed in cross section. These deviations from uniformity may develop during the coating process, as the result of deformation of the liquid/vapor meniscus by gravitational forces. The improved model, developed below, will be used to investigate the significance of these deviations. It will also be used to obtain diffusion coefficient estimates from columns that had coatings with slight irregularities.

In the previous study, the measured elution curves were nearly symmetric, and analysis using the method of moments provided reliable parameter estimates. However, for systems that exhibit lower diffusivity within the stationary phase, moment analysis becomes less attractive. At these conditions, the elution curves become skewed, with significant tailing. Calculation of the moments of skewed curves can result in significant errors, and the moment method becomes unreliable.

In this paper, we address this limitation by introducing an improved method of parameter estimation, based on analysis of temporal data transformed to the Fourier domain. To compare Fourier domain estimation to moment analysis, we first apply the new method to the same systems considered in part 1. The superiority of Fourier domain estimation is then demonstrated by an IGC study of methanol, methyl acetate, and methyl methacrylate in poly(methyl methacrylate). These systems, by virtue of their lower diffusivities, yield much more skewed elution curves, which preclude the effective use of moment analysis.

In part 1, all measurements were made at temperatures above the glass transition temperature of the polymer, and Fickian diffusion is expected. In part 2, measurements below the T_g have been investigated. At temperatures below the T_g, anomalous diffusion can occur if the diffusion Deborah number,[14] De, is of order unity; that is, the characteristic time for relaxation is approximately equal to the characteristic time for diffusion. De is not known for our IGC experiments. However, in the limit of an infinitely small concentration change, as approached in the IGC experiment at infinite dilution, the diffusion necessarily becomes Fickian, regardless of the value of De. As well, the diffusivity measured should be independent of De, since the state of the glass changes negligibly over the small concentration range of the IGC experiment. IGC effectively decouples the processes of transport and relaxation. Indeed, IGC may be more suitable for measuring the diffusivity of solvents in glassy polymers than the most commonly used experiment, sorption; the larger concentration range of the sorption experiment often results in relaxation of the glass and, hence, anomalous diffusion.

In this study, the capillary column IGC technique is demonstrated to be applicable at temperatures below the glass transition temperature; results of IGC measurements made on methanol in poly(methyl methacrylate) at temperatures below the T_g are reported and discussed.

Improved Model for Capillary Column Chromatography

In part 1,[1] the column was modeled as a straight capillary tube with an annular coating of uniform thickness. We now consider the case where the polymer coating is no longer a uniform film but exhibits some eccentricity when viewed in cross section. The nonuniform film model is presented as an extension to the uniform film model. For this reason, we begin by outlining the development of the transport equations for the uniform film case. A more detailed discussion of the uniform film model is found in part 1[1] and in the Pawlisch dissertation.[15]

Transport Equations for the Uniform Film Model. Following part 1, the same set of initial assumptions are used:

(1) The system is isothermal.

(2) The gas phase is treated as an incompressible fluid, since the axial pressure drop is small.

(3) The carrier flow is steady laminar flow with a parabolic velocity profile.

(4) The polymer phase is homogeneous.

(5) The polymer film is in the shape of a concentric annulus of constant thickness.

(6) The polymer film thickness is much less than the radius of the column.

(7) Axial diffusion in the stationary phase is negligible.

(8) The carrier gas is negligibly soluble in the polymer.

(9) The absorption isotherm is linear.

(10) Surface adsorption occurring at the polymer–gas interface and at the polymer–column interface is negligible.

(11) No chemical reaction occurs between the sample gas and the polymer.

(12) The diffusion coefficient varies negligibly over the small concentration variations of the IGC experiment.

(13) The injected sample enters the column as a narrow pulse so that the inlet concentration profile can be modeled as an impulse function.

In part 1, a description of the elution process was obtained by writing the continuity equation for the gas phase and the polymer phase. A complete solution of the problem requires that the gas-phase continuity equation be solved in two dimensions. However, for practical applications, the details of radial distribution of the solute are unimportant. A description of the longitudinal dispersion of the solute in terms of a radially averaged mean concentration is sufficient to describe the elution of a chromatographic peak. Thus, radial averaging was used to simplify the gas-phase equation. It was demonstrated

that, at the conditions of our experiments, the longitudinal dispersion of solute can be described by the following set of equations:

$$\frac{\partial \mathbf{c}}{\partial t} + V\frac{\partial \mathbf{c}}{\partial z} = D_g\frac{\partial^2 \mathbf{c}}{\partial z^2} + \frac{2D_p}{R}\frac{\partial c'}{\partial r}\bigg|_{r=R} \quad (1)$$

$$\frac{\partial c'}{\partial t} = D_p\frac{\partial^2 c'}{\partial r^2} \quad (2)$$

where V is the mean velocity of the carrier gas, z and r are the axial and radial coordinates, D_g and D_p are the gas-phase and polymer-phase diffusion coefficients, c' is the polymer-phase solute concentration, and $\mathbf{c}$ is the area-averaged gas-phase solute concentration, defined as

$$\mathbf{c} = \int_0^R rc\ dr \Big/ \int_0^R r\ dr \quad (3)$$

where c is the gas-phase concentration of solute and R is the distance from the center of the column to the polymer film.

The appropriate initial and boundary conditions are

$$\mathbf{c} = c' = 0 \quad \text{at} \quad t = 0 \quad (4)$$

$$\mathbf{c} = \delta(t)c_0 \quad \text{at} \quad z = 0 \quad (5)$$

$$\mathbf{c}(z,t) = c'(r,z,t)/K \quad \text{at} \quad r = R \quad (6)$$

$$\partial c'/\partial r = 0 \quad \text{at} \quad r = R + \tau \quad (7)$$

where c_0 is the strength of the inlet pulse, K is the partition coefficient, and τ is the film thickness.

In this formulation of the problem, transport of solute within the gas phase is modeled by using a plug-flow, convective-diffusion equation; transport of solute within the polymer phase is treated as diffusion in a slab. The equations are coupled via boundary conditions relating the transport and partitioning of solute between the two phases.

The key assumption required to derive eq 1 is that at any point within the column, radial concentration gradients within the gas phase are negligibly small. An equivalent statement is that the solute concentration in the gas phase is a very strong function of axial position but a very weak function of radial position. The assumption will be valid as long as radial diffusion, which tends to eliminate radial concentration gradients, occurs more rapidly than those processes that create radial concentration gradients (i.e., transport of solute between phases and the coupling of nonuniform axial convection with axial concentration gradients). As discussed by Pawlisch,[15] a plug-flow model can be justified for the experimental conditions used in this study.

The key assumption required to derive eq 2 is that the polymer coating is so thin relative to the radius of the column that the curvature of the film is negligible. Again, for the columns used in this study, the assumption is easily justified.[15]

Modification for Nonuniform Coatings. We now relax assumption 5 and modify eq 1 and 2 to deal with the case where the polymer film is not uniform. It will be assumed that the polymer film thickness varies only about the circumference of the column; the coating is still assumed to be uniform axially (i.e., in a cylindrical coordinate system (r, z, ϕ), the film thickness depends only on ϕ). Furthermore, we assume that the film retains an annular character (complete coverage of the wall) and that the variations in thickness occur gradually.

Because of the azimuthal variation in the film thickness, the solute flux across the gas–polymer interface is now a function of angular position. Because the problem is no longer axially symmetric, the gas-phase equation must be solved in three dimensions to obtain a full description of the solute distribution. However, in the previous model, we were able to use a one-dimensional description of gas-phase transport by assuming that radial concentration gradients are negligible.

We make a similar assumption in modeling the nonuniform case; concentration gradients normal to the axis of the column are considered to be negligibly small. Validity of the assumption again requires that transport processes normal to the column axis be rapid in comparison to axial convection and diffusion within the polymer phase. Note that the scaling of these transport processes is not fundamentally altered by allowing the coating thickness to vary slightly. Therefore, use of a nonuniform coating does not change the nature of solute transport within the gas phase. Consequently, eq 1 can still be used to model axial dispersion of the solute, provided that appropriate modifications are made to the boundary flux term. The point flux of solute, which is no longer independent of position, must be replaced by the solute flux averaged over the circumference of the column. That yields the following result:

$$\frac{\partial \mathbf{c}}{\partial t} + V\frac{\partial \mathbf{c}}{\partial z} - D_g\frac{\partial^2 \mathbf{c}}{\partial z^2} = \frac{2D_p}{R}\left\langle\frac{\partial c'}{\partial r}\right\rangle\bigg|_{r=R} \quad (8)$$

where R is now the average radius to the polymer–gas interface, and the broken brackets denote an average taken over the circumference, defined as

$$\langle f\rangle = \int_0^{2\pi} f(\phi)\ d\phi \Big/ \int_0^{2\pi} d\phi \quad (9)$$

When the film thickness varies with position, the polymer-phase continuity equation must be solved in three dimensions to obtain a full description of solute transport. However, in the previous model, axial diffusion in the polymer phase was assumed negligible on the basis of scaling considerations. That assumption is also valid in the present case.

It is further assumed that the film thickness changes very gradually with position. Because of this, azimuthal diffusion is also assumed to be negligible in comparison to radial diffusion. Locally, therefore, solute transport within the polymer phase is essentially one-dimensional, in a direction normal to the film surface. Consequently, transport in the polymer layer will continue to be treated as diffusion in a slab:

$$\frac{\partial c'}{\partial t} = D_p\frac{\partial^2 c'}{\partial r'^2} \quad (10)$$

with

$$c' = 0 \quad \text{at} \quad t = 0 \quad (11)$$

$$c' = \mathbf{c}K \quad \text{at} \quad r' = 0 \quad (12)$$

$$\partial c'/\partial r' = 0 \quad \text{at} \quad r' = \tau(\phi) \quad (13)$$

and where $r' = r - R$. Because of the boundary condition given as eq 13, the solution of the polymer transport equation is now a function of ϕ.

The problem is now made dimensionless by introducing the following variables:

$$q = \frac{c'L}{c_0VK} \qquad y = \frac{\mathbf{c}L}{c_0V} \qquad \theta = \frac{tV}{L} \quad (14)$$

$$\eta = r'/\tau_m \qquad x = z/L \qquad W(\phi) = \tau(\phi)/\tau_m$$

where τ_m is the mean film thickness, $\langle\tau(\phi)\rangle$, and $W(\phi)$ is the dimensionless film thickness.

In dimensionless form the transport equations become

$$\frac{\partial y}{\partial \theta} + \frac{\partial y}{\partial x} - \gamma \frac{\partial^2 y}{\partial x^2} = \frac{2}{\alpha \beta^2} \left\langle \frac{\partial q}{\partial \eta} \right\rangle \Bigg|_{r=R} \tag{15}$$

$$\frac{\partial q}{\partial \theta} = \frac{1}{\beta^2} \frac{\partial^2 q}{\partial \eta^2} \tag{16}$$

where

$$\alpha = \frac{R}{K\tau_m} \qquad \beta^2 = \frac{V\tau_m{}^2}{LD_p} \qquad \gamma = \frac{D_g}{VL} \tag{17}$$

The initial and boundary conditions become

$$y = q = 0 \quad \text{at} \quad \theta = 0, x > 0 \tag{18}$$

$$y = \delta(0) \quad \text{at} \quad x = 0 \tag{19}$$

$$q = y \quad \text{at} \quad \eta = 0 \tag{20}$$

$$\partial q/\partial n = 0 \quad \text{at} \quad \eta = W(\phi) \tag{21}$$

With use of Laplace transforms, eq 15–21 may be solved to obtain

$$Y(s) = \exp\left[\frac{1}{2\gamma}\right] \exp\left\{-\frac{1}{2\gamma}[1 + 4\gamma\Psi(s)]^{1/2}\right\} \tag{22}$$

where $\Psi(s)$ is given by

$$\Psi(s) = s + \frac{s^{1/2}}{\pi\alpha\beta}\int_0^{2\pi} \tanh\,[\beta s^{1/2} W(\phi)]\, d\phi \tag{23}$$

and where $Y(s)$ is the Laplace transform of the exit concentration, defined as

$$Y(s) = \int_0^\infty y(\theta, x=1) e^{-s\theta}\, d\theta \tag{24}$$

The transform (eq 23) cannot be inverted (analytically or numerically) until a film distribution function is specified. Even with very simple film distribution functions, the resulting transform may be more complex than for the uniform film case and, thus, not invertible analytically.

However, with the moment-generating property of Laplace transforms, general expressions for the moments of the real-time concentration distribution can be obtained without specifying a distribution function.

It is readily shown that

$$\mu_k = \left[\frac{L}{V}\right]^k (-1)^k \lim_{s\to 0} \frac{d^k Y(s)}{ds^k} \tag{25}$$

where

$$\mu_k = \int_0^\infty t^k \mathbf{c}(t)\, dt \Big/ \int_0^\infty \mathbf{c}(t)\, dt \tag{26}$$

The normalized moments can be used to calculate central moments, which are frequently more meaningful in characterizing an elution curve:

$$\mu_k{}^* = \int_0^\infty (t - \mu_1)^k \mathbf{c}(t)\, dt \Big/ \int_0^\infty \mathbf{c}(t)\, dt \tag{27}$$

Application of these equations to the Laplace transform solution yields the following set of moment equations:

$$\mu_1 = \left[\frac{L}{V}\right]\left\{1 + \frac{2}{\alpha}\right\} \tag{28}$$

$$\mu_2{}^* = \left[\frac{L}{V}\right]^2 \left\{\frac{2\beta^2}{3\pi\alpha}\int_0^{2\pi} W^3(\phi)\, d\phi + 2\gamma\left[1 + \frac{2}{\alpha}\right]^2\right\} \tag{29}$$

These equations are similar to those derived in part 1 and reduce to the uniform film case when $W(\phi) = 1$. As expected, the first moment or retention time of a sample is not dependent on the geometry of the coating. The second moment about the mean, or peak variance, is a function of the polymer phase diffusivity and the geometry of the coating. In general, nonuniformity of the coating will increase the variance of a chromatographic peak beyond what would be observed for a uniformly coated column. Consequently, application of a uniform film model to analyze data from an irregularly coated column will underestimate the diffusivity. The effect of coating irregularities on diffusion coefficient estimates is considered in greater detail below.

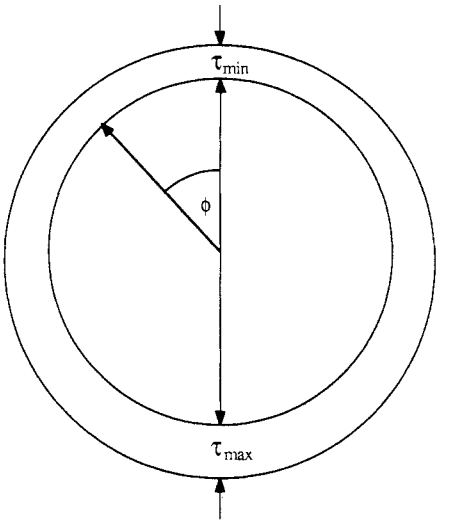

Figure 1. Cross-sectional drawing of a nonuniform coating. Diagram illustrates the nature of the film asymmetry observed in some columns. This film thickness is not to scale (with respect to the column radius) to make the nonuniformity more obvious.

Results for a Simple Distribution. Quantitative information about the effect of film irregularities on diffusion measurements requires that specific film distribution functions be considered. In this section, results for the simplest kind of nonuniform film are presented to show that minor variations in film thickness have a minimal effect on the accuracy of diffusion coefficient estimates.

The choice of film distribution function was motivated by the results of direct examination of column samples by using a scanning electron microscope. When viewed in cross section, all the samples showed annular coatings. However, in some columns, the coatings were asymmetric, having the appearance of an eccentric annulus, as shown in Figure 1. To model the coating, we assumed that the coating was symmetric about a line bisecting the annulus and that within each half-section, the film thickness is a linear function of angular position. That is

$$W(\phi) = a + b|\phi| \qquad -\pi < \phi < \pi \tag{30}$$

Because $W(f)$ is a normalized distribution function, the following must be true:

$$\frac{1}{\pi}\int_0^\pi W(\phi)\, d\phi = 1 \tag{31}$$

Because of this restriction, the film distribution function can be written as a one-parameter model in terms of either "a" or "b". Experimentally, however, it is more convenient to characterize the film uniformity by measuring the ratio of the thinnest to thickest film dimensions observed at a particular cross section. This ratio, designated Q_i, is related to the parameters "a" and "b" by the following:

$$a = \frac{2Q_i}{1 + Q_i} \qquad b = \frac{2(1 - Q_i)}{\pi(1 + Q_i)} \tag{32}$$

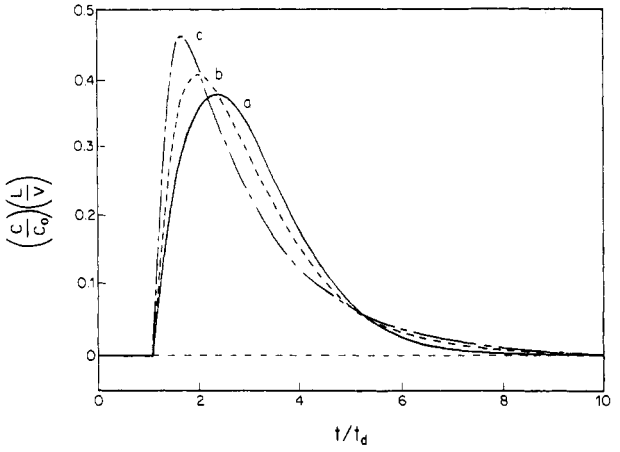

Figure 2. Effect of coating asymmetry on the elution profile. These theoretical profiles were obtained by using a nonuniform film model with $\alpha = 1$, $\beta = 1.0$, and $\gamma = 0.000\,01$; Q_i was varied to show the effect of film nonuniformity on peak shape. Curve a, with $Q_i = 1.0$, is for a uniform film. Curve b is for $Q_i = 0.25$, an intermediate degree of asymmetry. Curve c is for $Q_i = 0.0$, the most severe asymmetry possible.

where Q_i is τ_{min}/τ_{max}, "a" is τ_{min}/τ_m, and "b" is the slope of the film surface. Q_i is bounded by 0 and 1, with the latter representing a uniform film and the former representing the most severe asymmetry possible with this particular model.

For the simple film distribution, the integrals in eq 23 and 29 can both be evaluated analytically. Substitution of the film model into eq 23 yields the following transform:

$$Y(s) = \exp\left[\frac{1}{2\gamma}\right] \exp\left\{-\frac{1}{2\gamma}[1 + 4\gamma\Psi(s)]^{1/2}\right\} \quad (33)$$

where $\Psi(s)$ is given by

$$\Psi(s) = s + \left(\frac{2}{\alpha\beta^2\pi b}\right) \log\left[\frac{\cosh[\beta s^{1/2}(a + b\pi)]}{\cosh[\beta s^{1/2}a]}\right] \quad (34)$$

When axial molecular diffusion is negligible (i.e., $1/\gamma = 0$), then eq 33 simplifies to

$$Y(s) = \exp[-\Psi(s)] \quad (35)$$

Substitution of the film model into eq 29 yields the following expression for the variance of the elution curve:

$$\mu_2^* = \left[\frac{L}{V}\right]^2\left[\frac{4\beta^2}{3\alpha}\frac{2(1 + Q_i^2)}{(1 + Q_i)^2} + 2\gamma\left(1 + \frac{2}{\alpha}\right)^2\right] \quad (36)$$

This last result clearly shows the effect of film nonuniformity upon spreading of the elution curve. As the film changes from completely uniform to highly nonuniform (i.e., as Q_i decreases from 1 to 0), the magnitude of the first term in eq 36 doubles. Since the second term of eq 36 generally will be negligible when polymeric stationary phases are used, the variance of the resulting elution curve could be increased by as much as a factor of two. The qualitative effect of increasing film asymmetry on peak shape is illustrated in Figure 2. Shown are theoretical plots for three different values of Q_i, at fixed values for α and β. The general effect of film asymmetry is to skew the distribution more sharply.

It should be apparent from eq 36 and from Figure 2 that if a uniform film model is used to analyze experimental data obtained from a nonuniform film, then the estimated

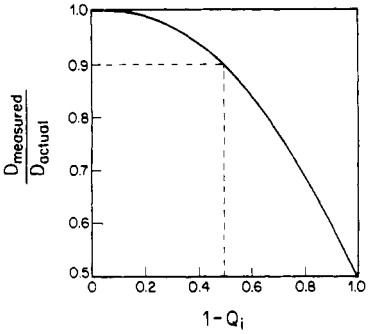

Figure 3. Sensitivity of the diffusion coefficient estimate to film uniformity. Diagram shows the error that results from using a uniform film model to calculate the diffusivity from elution curves obtained with an asymmetric coating.

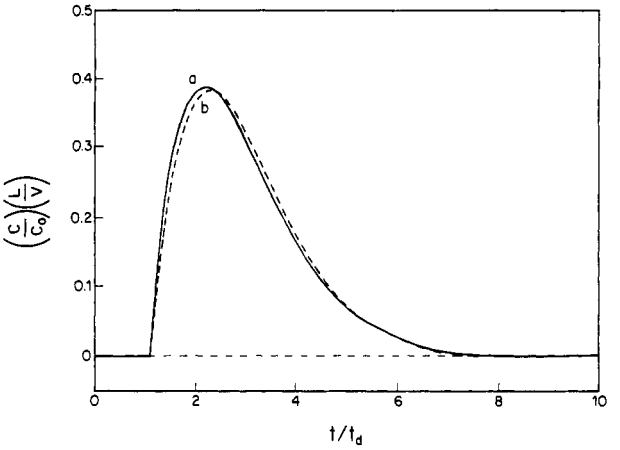

Figure 4. Effect of coating asymmetry on the elution profile with a low degree of film asymmetry. These theoretical profiles were obtained by using a nonuniform film model with $\alpha = 1.0$, $\beta = 1.0$, and $\gamma = 0.000\,01$. For curve a, $Q_i = 1.00$; for curve b, $Q_i = 0.5$.

value of the diffusivity will be lower than the correct value. For the case where moment analysis is used to obtain the diffusivity, the error that will result can readily be determined by comparing the second moment equations for the two models. The apparent or measured diffusivity (i.e., assuming a uniform film) is related to the true diffusivity and the film geometry by the following:

$$D_{measured} = D_{actual}\left[\frac{(1 + Q_i)^2}{2(1 + Q_i^2)}\right] \quad (37)$$

Figure 3 shows a plot of this relationship for the permissible values of Q_i. The peak variance is relatively insensitive to film asymmetry for moderately irregular films ($Q_i \geq 0.5$). As long as there are no sections of the film much thicker or thinner than the mean value, use of a uniform film model will not lead to significant errors in the estimated value of the diffusion coefficient. For example, when Q_i is 0.5, the value of D_p estimated with a uniform film model will only be 10% low. The relative insensitivity of peak shape to small irregularities in the film geometry is further illustrated in Figure 4, which compares theoretical elution curves for Q_i equal to 0.5 and 1.0, at a fixed value of α and β. The resulting curves are nearly identical in shape.

Increasing the film asymmetry has the same effect on the second moment as decreasing the polymer-phase diffusion coefficient; however, it affects the shape of the elution curve differently. This is illustrated by Figure 5, which compares theoretical elution curves for a uniformly coated and nonuniformly coated column, where the diffusion coefficients have been selected to yield identical

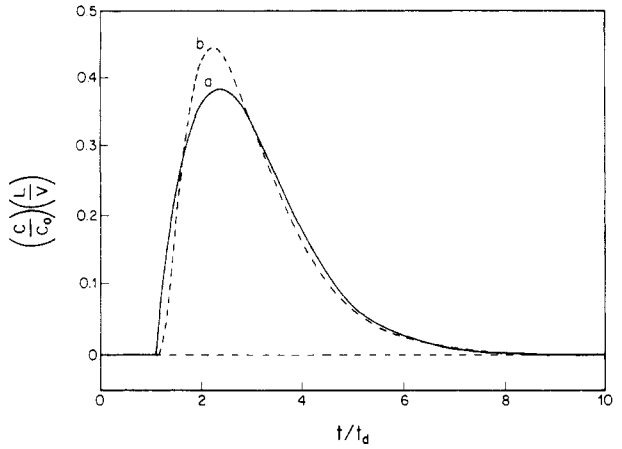

Figure 5. Comparison of the effects of coating asymmetry and polymer-phase transport resistance on the elution profile. These theoretical profiles have identical second moments but differ significantly in shape. Curve a was obtained for a uniform coating and a lower value of the diffusivity ($Q_i = 1.0$, $\beta = 1.0$, $D = D_0$). Curve b was obtained for an asymmetric coating and a higher value of the diffusivity ($Q_i = 0$, $\beta = 0.707$, $D = 2D_0$).

values for the second moments. Though the variance of each curve is the same, the elution curves are significantly different in appearance.

Estimation of Model Parameters. An IGC experiment is a classic example of an input–response experiment: the chromatogram (system response) is produced by injecting solute into the inlet of the column (an input disturbance). Methods for obtaining estimates of parameters in a mathematical model of a system from input–response experiments are well developed and generally fall into one of four categories: time domain estimation, Laplace domain estimation, Fourier domain estimation, and the "method of moments".[16]

In the first paper of this series,[1] moment analysis was used to obtain parameter estimates from experimental elution curves. The procedure is simple and direct. Experimental elution curves are first integrated to obtain first and second moments, as defined by eq 26 and 27. Then these results are used with eq 28 and 29 to calculate the diffusion and partition coefficient.

Moment analysis worked well in the previous study, because the elution curves were nearly symmetric, with well-defined end points. However, the method of moments have several well-known shortcomings that limit its use as a general analytical technique.[17]

The foremost difficulty is the nature of the weighting function used in eq 27. By virtue of the polynomial weighting function, experimental central moments will be strongly influenced by data collected far from the mean of the distribution. For pulse or peaklike distributions, these regions correspond to the tails of the elution curve, where the signal level and signal-to-noise ratio are small. The magnitude of higher order moments is increasingly sensitive to random signal fluctuations. Moreover, accurate calculation of higher order moments requires that the reference base line be well-defined and stable and that the end point of the elution curve is readily identified. If these conditions cannot be met, then large errors can result, either from truncation of the tail or from integration of noise in the base-line signal.

As a consequence of the increasingly poor accuracy of higher order moments, moment analysis is generally restricted to determination of one or two parameters. The procedure also does not admit discrimination between models, as the lower order (first and second) moments of a distribution provide a very limited characterization of peak shape; third moments, for example, are needed to test for the skewness. In addition, the method of moments does not provide an unequivocal criterion for the goodness of fit. To ensure that a good fit of the model has been attained, we find it is necessary to make a direct comparison of the original response curve with the theoretical response curve predicted by the parameter estimates.

Estimation in the time domain of the model parameters avoids these difficulties and is preferred for its increased accuracy and reliability. Parameters are selected to minimize an objective function that expresses, according to some specified criterion, the difference between the experimental and theoretical response curves.[18,19] Typically, a least-squares objective function is chosen. The key difficulty in applying time domain estimation to this application is that an analytical solution of the model equations in the time domain is not available. Thus, minimization of the objective function requires repetitive numerical computation of the theoretical response curve in the time domain.

A more attractive alternative to moment analysis is the estimation in the Fourier or Laplace domains. Although usually classified as different methods, Fourier and Laplace domain estimation are fundamentally the same because the properties and structure of the transforms are similar. In both methods, the transform of the experimental response curve is first generated numerically; the analytical expression for the transform is subsequently fitted directly to the transformed response curve by using a nonlinear regression algorithm.[20,21]

Of these alternatives to the method of moments, Fourier domain estimation was chosen for the current study. The key advantage of this technique is that an estimation criterion may be defined equivalent to a least-squares criterion in the time domain.[21] For those models that do not yield analytical time domain solutions, Fourier domain estimation is computationally more efficient and yields an equivalent result.

Estimation in the Fourier Domain. With Fourier domain estimation, model parameters are chosen to minimize the difference between the Fourier transforms of experimental and theoretical elution curves. The Fourier transform of a bounded, time-varying response curve, $f(t)$, is defined as

$$G(\omega) = \int_{-\infty}^{\infty} f(t)\, e^{-i\omega t}\, dt \tag{38}$$

If $f(t) = 0$ for $t < 0$, then substitution of $s = i\omega$ into the above equation yields the definition of the Laplace transform. Thus, the Fourier transform can be obtained from the Laplace transform solution (eq 22 and 23) by the substitution $s = i\omega$. The Fourier transform of an experimental elution curve can be calculated at discrete values of ω by numerical integration of eq 38. The specific algorithms used in this study are given later.

The best criterion for minimizing the difference between the theoretical and experimental transform is not immediately obvious. In the time domain, a least-squares criterion is usually preferred.[22] That is, parameters are selected that minimize the following objective function:

$$I = \int_{-\infty}^{\infty} \{f_t(t) - f_e(t)\}^2\, dt \tag{39}$$

where $f_e(t)$ is the experimental response curve, and $f_t(t)$ is the theoretical response curve.

It follows from Parseval's theorem that a least-squares criterion in the time domain is equivalent to the following criterion in the Fourier domain:[23]

$$I = \frac{1}{2\pi}\int_{-\infty}^{\infty}\{R_e(\omega) - R_t(\omega)\}^2 + \{I_e(\omega) - I_t(\omega)\}^2\, d\omega \quad (40)$$

where $R(\omega)$ denotes the real part of the Fourier transform, $I(\omega)$ denotes the imaginary part of the Fourier transform, and the subscript indicates an experimental or theoretical transform.

Because the transform of the experimental response curve must be evaluated numerically, eq 40 can only be evaluated numerically, over a finite interval. Approximating the integral by a finite sum over the interval $[-\Omega,\Omega]$ yields the following:

$$I = \sum_{n=-N}^{N}[\{R_e(\omega_n) - R_t(\omega_n)\}^2 + \{I_e(\omega_n) - I_t(\omega_n)\}^2]\Delta\omega/(2\pi) \quad (41)$$

where $\Delta\omega = \Omega/N$, and $\omega_n = n\Delta\omega$.

The accuracy of this approximation is dependent on both the size of the interval and the number of partition points. Use of a partial integral to approximate the Fourier transform is analogous to truncation of the higher order terms of a Fourier series expansion. For the response curves obtained in an IGC experiment, the magnitude of the Fourier transform approaches 0 for large ω. Thus, the truncation error associated with eq 41 can be made as small as directed simply by increasing Ω.

For reasons that will become apparent, it is convenient to redefine the size of $\Delta\omega$ in terms of the duration of the elution curve. Suppose that the elution curve, $f(t)$, is recorded for the time interval $(0,t_m)$, where t_m is sufficiently large that $f(t)$ may be assumed to be 0 outside of the interval. Then we define the partitioning of the frequency domain as

$$\omega_n = n\pi/t_m \quad (42)$$

Substituting this definition into eq 41 and utilizing the fact that $G(-\omega)$ equals the complex conjugate of $G(\omega)$ yield the following result:

$$I = \frac{1}{2t_m}[\{R_e(0) - R_t(0)\}^2 + \{I_e(0) - I_t(0)\}^2] + \frac{1}{t_m}\sum_{n=1}^{N}[\{R_e(\omega_n) - R_t(\omega_n)\}^2 + \{I_e(\omega_n) - I_t(\omega_n)\}^2] \quad (43)$$

Minimization of this function with respect to the unknown model parameters results in the best least-squares approximation of the experimental elution curve in the time domain.

Note that by using the definition of the Fourier transform and taking into account the properties of $f(t)$, we may obtain the following:

$$R(\omega) = \mathrm{Re}\{F(\omega)\} = \int_{-\infty}^{\infty} f(t)\cos(\omega t)\, dt$$

$$R(\omega_n) \cong \int_0^{t_m} f(t)\cos(\omega_n t)\, dt = t_m A_n \quad (44)$$

$$I(\omega) = \mathrm{Im}\{F(\omega)\} = -\int_{-\infty}^{\infty} f(t)\sin(\omega t)\, dt$$

$$I(\omega_n) \cong \int_0^{t_m} f(t)\sin(\omega_n t)\, dt = t_m B_n \quad (45)$$

where A_n and B_n are the coefficients of a Fourier series expansion of $f(t)$ over the time interval $(-t_m,t_m)$. Thus, eq 43 is computationally equivalent to evaluating the sum of the squared differences between corresponding Fourier series coefficients of the theoretical and experimental response curve. The approximation errors associated with eq 43 are related to the convergence properties of these Fourier series expansions.

In the present study, eq 43 with 200 series coefficients (i.e., the summation truncated at $N = 99$) was used as the objective function in the estimation of the unknown model parameters. As discussed earlier, values for the theoretical Fourier transform were obtained by substituting $s = i\omega$ into the Laplace transform solution. Experimental transform values were obtained by numerical integration of eq 44 and 45, by using a trapezoidal rule algorithm.

Selection of the best set of model parameters was done by using a commercial nonlinear regression code (subroutine ZXSSQ from the IMSL software library, International Mathematical & Statistical Libraries, Inc., Houston, TX). This code is based on a Levenberg–Marquardt algorithm and returns estimates of α and β precise to four digits. Generally, initial guesses for α and β were obtained via moment analysis.

The number of coefficients used in the fitting routine is limited by the need to evaluate the experimental series coefficients by numerical integration. Because the integrand contains an oscillatory function, some caution is required when a trapezoidal rule is used to evaluate the integral. Unless the period of oscillation of the integrand is much longer than the sampling period of $f(t)$, the approximation of the integral obtained by an interpolatory quadrature rule will be poor. This restricts the use of trapezoidal rule integration to small values of ω_n. In practice, this is not a severe limitation. Both the real and imaginary parts of $G(\omega_n)$ approach 0 as n becomes large; the higher frequency coefficients contribute little to the objective function and thus have little effect on the minimization procedure.

Table I
Summary of Column Dimensions

	polystyrene			PMMA	
	col 1	col 2	col 3	col 1	col 2
coating solvent	THF	THF	chloroform	chloroform	MEK
film thickness, μm	11.7	6.7	9.0	6.3	5.3
inner radius of column, μm	629.0	669.0	563.0	426.0	367.0
axial length of column, m	14.96	15.63	15.62	16.70	17.78

Experimental Section

The apparatus and general procedures of the capillary column IGC experiment were described in part 1[1] and will not be repeated here.

Materials. The characteristics of the polymer and solvents used for the polystyrene work were described in part 1. The PMMA used in this study was a commercial grade (PRD-41) manufactured by the Rohm and Haas Co. The PMMA had a weight-average molecular weight of 200 000 and a polydispersity of 2.35 (determined by gel permeation chromatography). The glass transition temperature of the PMMA was 116–120 °C, as measured by differential scanning calorimetry. Methanol, methyl acetate, and methyl methacrylate were of spectral grade products, obtained from MCB Manufacturing Chemists Inc. (a division of EM Industries, Inc., Gibbstown, NJ).

Column Preparation. The preparation of the three columns used for the polystyrene work was described in detail in part 1. For convenient reference, the physical characteristics of the three columns are summarized in Table I. The average film thickness and average interior diameter were determined indirectly, via measurements of the column weight, the coating weight, and the outside diameter of the column.[1] The uniformity of the coating was evaluated by examining numerous samples of each column with a scanning electron microscope.[15] Micrographs of cross sections taken at several points along the length of each column showed the coating to be annular in character, with complete coverage of the column wall and a high degree of axial uniformity.

With columns 1 and 3, coatings were uniform in thickness. The coating in column 2 was slightly asymmetric with respect to the axis of the column. The coating edge had the appearance of an eccentric annulus, as illustrated by Figure 1. The ratio of minimum coating thickness to maximum coating thickness, Q_i, was about 0.6 for all of the samples examined. The asymmetry in the coating is thought to result during the coating process from deformation of the liquid–vapor interface by gravity.

Two columns were coated with PMMA by using the static coating method described in part 1. The average film thicknesses and column dimensions are summarized in Table I. The dimensions of column 1 were measured by using the destructive characterization technique, presented in part 1. Column 2, however, was not destroyed to measure the film thickness; rather, the film thickness was inferred from values of α and β measured on column 2 and from the values of the diffusivity and partition coefficient measured on column 1 at the same temperature. From the definitions of α and β in eq 17 and from the measured values of the diffusivity and partition coefficient, the film thickness was estimated. Column 1 exhibited a slight eccentricity with a value of Q_i of approximately 0.7.

Data Reduction. The theoretical model was fit to each elution curve to obtain an estimate of α and β by using the Fourier estimation procedure. The partition coefficient and diffusion coefficient were then calculated from α and β, by using average coating and column dimensions. The measure of axial dispersion γ was negligibly small for all of the experiments, so the simpler form of the theoretical transform solution (eq 34) was used. The Laplace transform solution developed for the case of a nonuniform coating (eq 35) was used to accommodate columns with slightly asymmetric coatings.

To quantify the goodness of fit, we used estimated values of α and β to generate a theoretical elution profile, by numerical inversion of the transform.[15] The inversion routine was programmed to output concentrations at times corresponding to the experimental data points. The agreement between the two curves was then quantified by calculating the sum of the squared differences between the two sets of data. The maximum difference between the two sets of curves, expressed as a percentage of the maximum concentration, was also determined.

Results and Discussion

Polystyrene Data. In part1,[1] capillary column IGC was used to measure the partition coefficient and diffusion coefficient of benzene, toluene, and ethylbenzene in polystyrene, from 110 to 140 °C. In that study, moment estimation was used to obtain parameter estimates from the elution curves. In this paper, the same experimental data (elution curves) are reanalyzed by using Fourier domain estimation. The primary purpose of this exercise is to provide a direct comparison of the two estimation methods. A comparison of the IGC results with previous literature was given in part 1, and will not be repeated here.

As outlined in part 1, measurements for each solvent/polymer pair were obtained at several carrier flow rates, with use of each of the three columns described in Table I. Table II contains a summary of the experimental conditions used in the study. In the discussion that follows, all experiments within a row of Table II will be referred to as a data set. Note that two or three replicate elution curves were obtained at each of the conditions listed, and all measurements were made at conditions approaching infinite dilution of the solvent. The use of multiple columns and several flow rates was intended to provide for checks of the validity of the theoretical model used for the analysis.

Estimates of α and β were obtained for each elution curve by using the Fourier estimation procedure outlined earlier. To confirm that a satisfactory fit between model and experiment had been obtained, we used the parameter estimates to generate theoretical elution curves, via numerical inversion of the Laplace transform solution. In every case, the theoretically generated curve accurately reproduced the original elution curve. The maximum deviation between the theoretical and experimental elution curves ranged from 3% to 6% of the peak value of the elution curve.

Table II
Summary of Experimental Conditions of PS Study

solvent	temp, °C	col	approx carrier velocity, cm/s			
benzene	110.0	2	2.00	2.65	4.10	
	120.1	1	2.65	3.50	5.00	
	120.2	2	3.20	4.60	7.65	
	130.2	1	3.20	5.00	9.25	
	130.4	2	4.25	6.00	7.30	8.80
	130.2	3	5.50	7.80	14.40	24.60
	140.6	2	5.35	7.60	11.80	
toluene	110.0	2	2.00	2.65	4.10	
	120.1	1	2.65	3.50	5.00	
	120.2	2	3.20	4.60	7.65	
	130.2	1	3.20	5.00	9.25	
	130.4	2	4.25	6.00	7.30	8.80
	130.2	3	5.50	7.80	14.40	24.60
	140.6	2	5.35	7.60	11.80	
ethylbenzene	110.0	2	2.00	2.65	4.10	
	120.1	1	2.65	3.50	5.00	
	120.2	2	3.20	4.60	7.65	
	130.2	1	3.20	5.00	9.25	
	130.4	2	4.25	6.00	7.30	8.80
	130.2	3	5.50	7.80	14.40	24.60
	140.6	2	5.35	7.60	11.80	

Evaluation of the Model. Within each data set, tests were performed to verify that the results showed the proper dependence on carrier velocity.

The dimensionless parameter α depends only on the partition coefficient and coating thickness. Thus, according to the model, α should not be dependent on carrier velocity. This was observed experimentally; within a data set, values of α were essentially constant. In the worst cases (experiments with column 2 at 120 and 130 °C), the maximum deviation of any individual measurement from the mean value of the data set did not exceed 6%. In at least half of the data sets, the maximum deviation from the mean was less than 2%. Standard statistical tests showed no significant correlation of α with flow rate (at a 90% confidence level) for the majority of the data. The exceptions to this were the data from column 2 at 140 °C and the data for ethylbenzene at 120 °C from column 1. However, for each of these data sets, the value of α was constant to ±2%; this variation is so small that no physical significance is attributed to the observed correlation.

The dimensionless parameter β^2 is inversely proportional to the carrier residence time, t_d. Thus, according to the model, the quantity $\beta^2 t_d$ should not be dependent on carrier velocity. This was observed experimentally; within a given date set, the value of $\beta^2 t_d$ was essentially constant. In the worst case, the data for benzene at 130 °C from column 2, the maximum deviation of an individual measurement from the mean value of the data set was only 10%. In the majority of the other data sets, individual measurements did not deviate from the mean by more than 5%. Tests of the correlation coefficient for plots of $\beta^2 t_d$ versus $1/t_d$ show no significant correlation (at a 90% confidence level) for the majority of the data sets. In all cases where the test indicated statistical significance of the correlation, the maximum variation in the value of $\beta^2 t_d$ is less than 4%. This variation is so small that no physical significance is attributed to the correlation.

Summary of Fourier Estimation Results. Table III gives a summary of the Fourier estimation results. For later comparison, the moment analysis estimates from part 1 are also shown. The number in parentheses following

Table III
Comparison of Results Derived by Moment and Fourier Analysis for PS Study

			Fourier method		moments method	
solvt	temp, °C	col	partition coeff (σ)	diffusivity, 10^{10} cm^2/s (σ)	partition coeff (σ)	diffusivity, 10^{10} cm^2/s (σ)
benzene	110.0	2	40.9 (0.9)	9.32 (0.32)	42.6 (0.9)	7.84 (0.41)
	120.1	1	33.6 (1.2)	29.80 (1.7)	33.7 (1.2)	28.20 (1.7)
	120.2	2	34.2 (1.2)	31.10 (1.0)	35.5 (1.5)	23.70 (1.6)
	130.2	1	26.9 (0.9)	98.30 (5.6)	27.0 (0.9)	96.60 (5.7)
	130.4	2	27.1 (0.8)	90.70 (3.4)	27.5 (0.7)	84.80 (3.7)
	130.2	3	26.8 (0.6)	97.70 (3.1)	26.7 (0.6)	93.10 (3.8)
	140.6	2	21.8 (0.9)	258.00 (9)	22.1 (0.8)	253.00 (12)
toluene	110.0	2	82.8 (2.2)	4.34 (0.16)	86.0 (3.9)	3.60 (0.2)
	120.1	1	63.7 (2.2)	16.10 (0.93)	63.7 (2.2)	15.80 (0.9)
	120.2	2	64.5 (2.8)	16.70 (0.62)	66.1 (3.4)	14.20 (1.0)
	130.2	1	49.4 (1.7)	61.20 (3.5)	49.5 (1.7)	59.30 (3.8)
	130.4	2	49.9 (1.3)	58.30 (1.9)	50.8 (1.5)	54.10 (3.0)
	130.2	3	50.4 (1.1)	61.40 (1.8)	50.6 (1.3)	60.10 (2.3)
	140.6	2	38.5 (0.9)	171.00 (6)	38.7 (0.9)	166.00 (6)
ethylbenzene	110.0	2	148.1 (6.1)	1.79 (0.06)	153.1 (7.8)	1.57 (0.12)
	120.1	1	109.2 (3.8)	8.00 (0.46)	108.7 (3.8)	8.04 (0.47)
	120.2	2	109.9 (2.0)	8.63 (0.30)	113.4 (2.3)	7.30 (0.26)
	130.2	1	82.9 (2.8)	33.90 (1.9)	83.2 (3.1)	33.00 (2.1)
	130.4	2	83.1 (2.2)	32.90 (1.1)	83.9 (2.5)	31.60 (1.5)
	130.2	3	84.0 (1.7)	35.30 (1.1)	83.6 (2.1)	37.30 (1.6)
	140.6	2	64.0 (1.5)	107.50 (3.8)	64.1 (1.5)	104.80 (3.8)

each table entry is an estimate of the standard deviation of the measurement, based on the accuracy of the column dimensions used in the calculations and the reproducibility of the measurement.

The partition coefficients reported in Table III were calculated from the mean value of α for each data set. Comparison of the entries at 120 and 130 °C show that the column to column reproducibility of the data is good. The difference between the measurements on different columns is consistent with the estimated standard deviation of the measurements. This agreement would also suggest that surface adsorption must have been negligible in the experiments.

The diffusion coefficients reported in Table III were obtained from each data set by plotting β^2 versus $1/t_d$. According to the model neglecting axial dispersion, this plot should be linear, extrapolate through the origin, and have a slope equal to τ_m/D_p. A linear least-squares fit of the data, constrained to pass through the origin, was used to obtain the slope. Comparison of the entries at 120 and 130 °C shows that the column to column reproducibility of the data is good. The difference between the measurements on different columns is consistent with the estimated standard deviation of the measurements.

Comparison of Moment and Fourier Estimation. Comparison of the data in Table III shows that the parameter estimates obtained by the method of moments are not significantly different from those obtained by Fourier domain estimation.

The agreement between partition coefficient estimates obtained by each method is excellent. With the exception of the 110 °C data, the partiion coefficient estimates for corresponding data sets differ by less than 3%. Since the estimated standard deviation of the measurements is typically 2–4%, the two sets of data are equivalent within experimental error.

The agreement between the diffusion coefficient estimates obtained by each method is also good, overall. In the majority of the cases, the estimates obtained for corresponding data sets differ by less than 5%. The exceptions to this were the results at 110 and 120 °C from column 2. In these cases, the estimates from moment and Fourier domain estimation are as much as 30% different, an amount greater than the estimated experimental error.

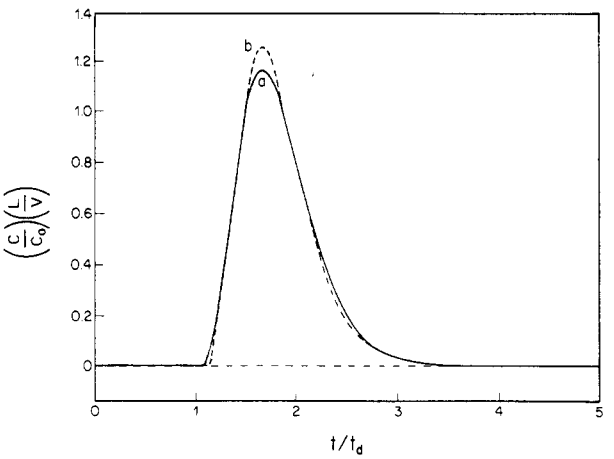

Figure 6. Comparison of a theoretical (a) and experimental (b) elution curve for benzene in PS from column 2 at 130 °C and a carrier velocity of 6 cm/s. The theoretical profile was generated by using the best set of parameters obtained by moment estimation. See Figure 7 for a comparison of the same experimental curve to the theoretical curve predicted for parameters estimated in the Fourier domain.

The larger disagreement that exists between these sets of data is probably the result of systematic errors in the moment data. In all of these cases, the diffusivity obtained from moment analysis is smaller than that obtained by Fourier domain estimation. It is further apparent, from a comparison of the other data sets, that the diffusivity determined by Fourier domain estimation is normally larger than the diffusivity determined by moment estimation. These observations would be consistent with systematic overestimation of the peak variance, as determined by integration of the elution curves. As discussed earlier, such errors are likely because of the nature of the weighting function used to calculate the second moment.

This explanation is supported by a comparison of theoretical and experimental elution curves to determine which set of parameters best reproduces the original elution curves. Such a comparison is shown in Figures 6 and 7, for the benzene data from column 2 at 130 °C. (The disagreement between the two methods of analysis was greatest for this data set.) As can be seen from the dia-

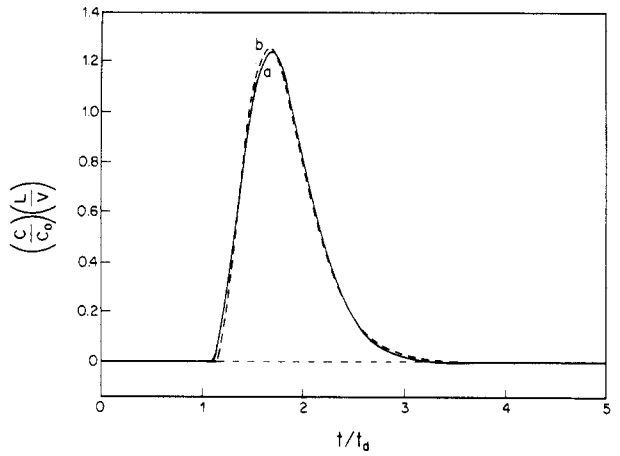

Figure 7. Comparison of a theoretical (a) and experimental (b) elution curve for benzene in PS from column 2 at 130 °C and at a carrier velocity of 6 cm/s. The theoretical profile was generated by using the best set of parameters obtained by Fourier domain estimation.

Table IV
Summary of Experimental Conditions of PMMA Study

solv	temp, °C	col	approx carrier velocity, cm/s		
MMA	135.5	1	14.22	7.81	3.52
	150.9	1	14.60	8.04	3.65
	161.1	1	15.00	8.28	3.71
MeAc	125.3	2	18.62	10.26	4.71
	135.5	2	18.88		4.75
	150.9	2	19.54	10.87	4.94
	161.0	2	20.07		5.11
MeOH	89.8	1	12.75	7.01	3.16
	100.3	1	12.88	7.12	3.21
	109.7	1	13.47	7.37	3.31
	125.2	1	13.74	7.63	3.46
	130.4	1	13.94	7.61	3.51
	135.4	1	14.13	7.87	3.52
	150.6	1	14.57	8.10	3.71
	160.8	1	14.84	8.28	3.76
	170.8	1	15.17	8.41	3.81
MeOH	125.2	2	18.46	10.23	4.69
	135.5	2	18.90	10.46	4.75
	150.7	2	19.58	10.95	4.96

grams, the parameters determined by Fourier domain estimation more closely reproduce the original elution curve.

The greater reliability of Fourier domain estimation can also be seen by comparing the column to column variability of results obtained by each method. For both the partition coefficient and diffusion coefficient, the Fourier estimation results are less variable than the moment estimation results.

Poly(methyl methacrylate) Data

Overview. The objective of this study was to extend the capillary column IGC technique to a second polymer stationary phase, to investigate the utility of the technique in studying polymer/solvent systems that exhibit highly skewed elution curves, and to determine if the capillary column IGC technique can be applied at temperatures below the glass transition temperature of the polymer.

The capillary column IGC technique was used to measure the partition coefficients and diffusion coefficients of methanol (MeOH), methyl acetate (MeAc), and methyl methacrylate (MMA) in poly(methyl methacrylate) (PMMA). Table IV contains a summary of the experimental conditions of each run. For each temperature, measurements were made at three different flow rates (two series of runs were made at only two flow rates), and at each flow rate, two or three replicate elution curves were obtained. All measurements were made at solute concentrations approaching infinite dilution.

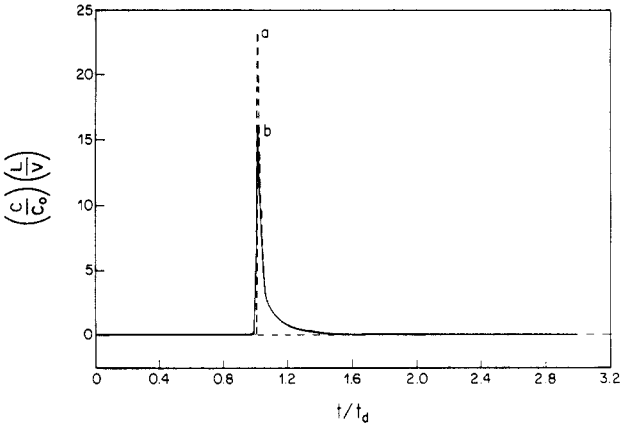

Figure 8. Comparison of highly skewed theoretical (a) and experimental (b) elution curves for MMA in PMMA at T = 135.5 °C.

Comparison of Moment and Fourier Estimation. In the polystyrene study discussed previously, the Fourier estimation technique was shown to give a slight improvement in the precision of the parameter estimation as compared with that of the moment estimation technique; however, the polystyrene elution curves exhibit a nearly Gaussian shape, and moment estimation is adequate for parameter estimation. The merits of Fourier estimation are expected to be evident when analyzing highly skewed elution curves. For these curves, the moment estimation technique yields significant errors due to the disproportionate weighting of the less reliable data in the long tail.

Skewing of elution curves increases with decreasing diffusivity. This can be explained by the reduction in the sorption and desorption rates of solute with decreasing diffusivity. For a low-diffusivity solute, the bulk of the solute remains in the gas phase, as only small amounts of the solvent can diffuse into the polymer phase. The result is a sharp spike of solute exiting with a residence time close to that of the carrier gas. After this spike passes, the solvent absorbed in the polymer slowly bleeds from the film, resulting in a long, flat tail. An experimental elution curve exhibiting these traits is shown in Figure 8 for MMA in PMMA at T = 135.5 °C.

PMMA was chosen as the stationary phase, since diffusion in PMMA is slower than in polystyrene. The elution curves are also more skewed. Comparison of results derived by moment estimation with those derived by Fourier estimation reveal that the Fourier estimation technique offers a significant improvement in the precision of the parameter estimates for all the systems studied. This improvement in precision was exhibited by an improved reproducibility of the model parameters, α and β, measured for replicate runs. In addition, the flow rate dependence of the model parameters determined by using the Fourier technique compared more favorably with that predicted by the model. In Figure 9, the dimensionless second central moment, μ^{*2}/t_d^2, calculated from values of α and β estimated by both the moment and Fourier techniques, are plotted versus $1000/t_d$ for MeOH at 160.8 °C. The improvement in both the reproducibility and the flow rate dependence of the data fit by the Fourier technique is evident (the model predicts a line through the origin). Similar improvements were evident for measurements on MeOH at all temperatures. In fact, the moment technique was unacceptable for analyzing MMA and MeAc data due to the greater skewing in their elution

Table V
IGC Results from PMMA Study

solvt	temp, °C	$1/T$, 10^3 K^{-1}	col	partition coeff	activity coeff	retention vol, cm^3/g	χ parameter	diffusivity, cm^2/s
MeOH	89.8	2.76	1	28.56	15.11	18.78	1.23	1.78×10^{-9}
	100.3	2.68	1	19.81	15.97	12.72	1.27	3.14×10^{-9}
	109.7	2.61	1	14.80	16.54	9.31	1.29	6.02×10^{-9}
	125.2	2.51	1	10.28	16.24	6.26	1.14	1.62×10^{-8}
	125.2	2.51	2	9.70	17.22	5.90	1.30	1.58×10^{-8}
	130.4	2.48	1	8.68	17.10	5.23	1.29	2.10×10^{-8}
	135.4	2.45	1	8.55	15.57	5.09	1.18	2.82×10^{-8}
	135.5	2.45	2	8.35	15.91	4.97	1.20	2.94×10^{-8}
	150.6	2.36	1	6.72	14.57	3.89	1.08	7.37×10^{-8}
	150.7	2.36	2	6.72	14.55	3.88	1.08	7.23×10^{-8}
	160.8	2.30	1	5.84	13.91	3.31	1.01	1.19×10^{-7}
	170.8	2.25	1	5.04	13.59	2.81	0.96	1.81×10^{-7}
MMA	135.5	2.45	1	31.04	5.14	18.49	0.31	9.13×10^{-11}
	150.9	2.36	1	14.93	7.91	8.63	0.72	1.25×10^{-9}
	161.1	2.30	1	13.74	7.16	7.79	0.60	3.14×10^{-9}
MeAc	125.3	2.51	2	13.36	6.25	8.13	0.46	4.23×10^{-10}
	135.5	2.45	2	8.75	7.97	5.22	0.68	2.05×10^{-9}
	150.9	2.36	2	7.36	7.40	4.25	0.58	8.57×10^{-9}
	161.0	2.30	2	6.52	7.20	3.70	0.53	1.47×10^{-8}

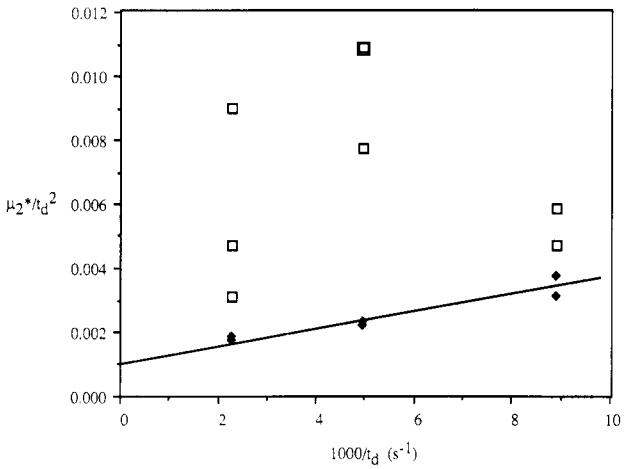

Figure 9. Comparison of the dimensionless second central moments determined by moment (□) and Fourier (◆) estimation for MeOH in PMMA at 160.8 °C.

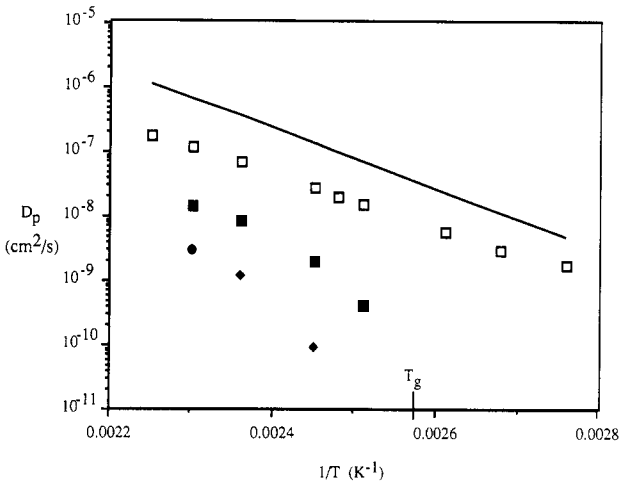

Figure 10. Temperature dependence of the infinite dilution diffusion coefficient of solute in PMMA: (□) MeOH; (■) MeAc; (◆) MMA. The solid line gives super-T_g data of MeOH in PMMA from Zhurkov and Ryskin.[26]

curves. For these solutes, only Fourier estimation gave acceptable reproducibility and flow rate dependence of the model parameters.

Diffusivity Measurements. Values of the diffusivities measured for MeOH, MeAc, and MMA in PMMA are listed in Table V. The ordering of the diffusivities is as expected with the smallest molecule, MeOH, exhibiting the largest diffusivity and the largest molecule, MMA, exhibiting the smallest diffusivity. In Figure 10, log D_p is plotted versus the reciprocal temperature for MeOH, MMA, and MeAc. The MeOH curve is linear, whereas a significant curvature is noticed for MeAc and MMA as the glass transition is approached. This behavior is consistent with that predicted by the free-volume theory of diffusion,[24] which predicts that the curvature increases as the glass transition temperature is approached. Free volume theory also predicts the curvature to increase with increasing volume of the penetrant molecule; this is also consistent with our measurements, as is evident in Figure 10.

A more appropriate analysis of the data in terms of free volume theory is to plot the log D_p versus $1/(K_{22} + T - T_g)$; K_{22} characterizes the free volume of the polymer and is discussed in detail by Vrentas and Duda.[24] This plot should be linear above and below the T_g. If excess free volume is frozen into the glass, a break in the slope is predicted at the T_g.

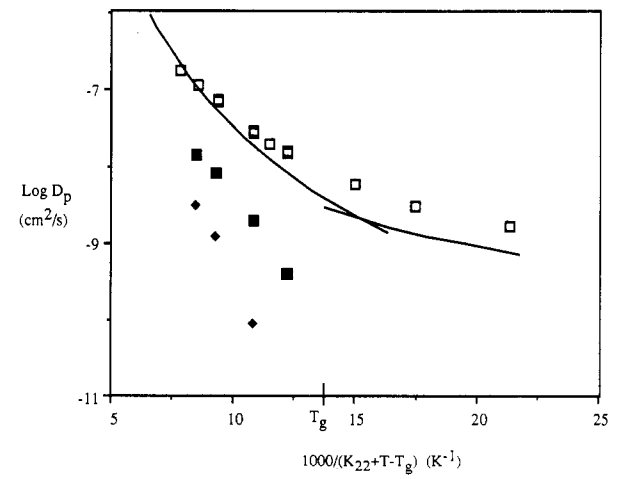

Figure 11. Free-volume plot of the infinite dilution diffusion coefficient of solute in PMMA: (□) MeOH; (■) MeAc; (◆) MMA. Solid lines give super-T_g and sub-T_g data of MeOH in PMMA from Zhurkov and Ryskin.[26]

In Figure 11, log D_p is plotted versus $1000/(K_{22} + T - T_g)$ for MeOH, MMA, and MeAc in PMMA. The value of K_{22} for PMMA was taken to be 73.0 K as given by Hu and Han.[25] Measurements were made both above and below the T_g for MeOH only. The MeOH plot is linear

above and below the glass transition with a break in the slope at or near the T_g (116 °C); this suggests that excess free volume was frozen into the polymer. The super-T_g plots for MMA and MeAc exhibit a slight downward curvature. Similar curvature is exhibited in plots for ethylbenzene, toluene, and *n*-decane in PMMA, as measured by Hu and Han[25] using a packed column IGC technique.

Comparison with Literature Data above T_g. For the penetrants investigated in this study, super-T_g diffusivity data are available only for MeOH. Zhurkov and Ryskin[26] measured the diffusivity of MeOH in PMMA using a vapor sorption technique. In Figure 10, Zhurkov and Ryskin's diffusivity data are also plotted for comparison with the diffusivity data of this study. Their data are presented as an Arrhenius plot defined by the relation $D_p = D_0 \log(-E_a/RT)$; Zhurkov reported values of E_a equal to 21.6 kcal/mol and D_0 equal to 50 118 cm^2/s at temperatures above the T_g. Their diffusivities vary from 2.5 to 6 times greater than those measured in our studies. The value of the super-T_g activation energy for MeOH measured in our study, 19.8 kcal/mol, is consistent with the value reported by Zhurkov.

The PMMA used by Zhurkov and Ryskin exhibits its T_g at about 87 °C, 31 °C below that of the PMMA used in this study. For comparison of these measured diffusivities on the basis of free-volume theory, the log of the diffusivities measured in both studies is plotted versus $1000/(K_{22} + T - T_g)$ in Figure 11. Although the values of the diffusivities agree more closely when plotted versus $1/(K_{22} + T - T_g)$, significant differences still exist. The disagreement is likely a result of the differences in the nature of the polymers, as suggested by the large differences in T_g values for the two PMMA's studied.

Comparison with Literature Data below T_g. The sub-T_g diffusion of MeOH in PMMA occurring in our IGC experiments is assumed to be Fickian, as changes in the state of the glass during the sorption process are expected to be negligible. This is explained by the small variation of the penetrant concentration attending the sorption process, a result of the small injection volumes (0.01 μL of liquid) used in the IGC technique.

Zhurkov and Ryskin[26] also measured diffusivities of MeOH in PMMA at temperatures below the glass transition. As for the super-T_g measurements, comparison of diffusivities will be made on the basis of the distance from the T_g to account for the lower T_g of Zhurkov and Ryskin's PMMA. In Figure 11, the log of the sub-T_g diffusivity measured in both studies is plotted versus $1/(K_{22} + T - T_g)$. The sub-T_g diffusivity data of Zhurkov presented in Figure 11 were calculated from the Arrhenius relation with E_a equal to 12.4 kcal/mol and D_0 equal to 0.1 cm^2/s, as reported by Zhurkov and Ryskin.[26] The sub-T_g plots exhibit a similar slope; however, the diffusivities measured in this study exceed those of Zhurkov's study by a factor of approximately 2.5.

Sub-T_g measurements of the diffusivity of MeOH, MMA, and MeAc in PMMA have been made by other investigators at a temperature of 30 °C. To compare them with the diffusivities measured in this study, we have extrapolated our plots of log D_p versus $1/T$ to 30 °C. The diffusivities measured by these investigators and our extrapolated values are listed in Table VI, along with the concentration ranges of the experiments. Hopfenberg et al.[27] measured the diffusivity of MMA in PMMA at 30 °C using a vapor sorption technique. Their value of the diffusivity is nearly 3 orders of magnitude larger than our extrapolated value. This is not surprising, however, as much larger diffusivities are expected at the high penetrant concentration (0.09 mass fraction) used in Hopfenberg's experiments. Also, contributions from case II transport, as reported in Hopfenberg's studies, further muddle the comparison. The diffusivity of MeAc in PMMA was measured by Wang and Kwei[28] using vapor sorption at 30 °C and at a penetrant mass fraction of 0.005. Close agreement is noted with our extrapolated value of the diffusivity. Berens and Hopfenberg[29] measured the diffusivity of MeOH in PMMA at 30 °C and at a penetrant mass fraction of 0.005, also using a vapor sorption technique. The diffusivity measured by using vapor sorption is twice as large as that measured by using IGC. Again, this is not unreasonable considering the finite concentration of the vapor sorption studies.

Table VI
Comparison of Sub-T_g Diffusivities of This Study Extrapolated to 30 °C with Values from the Literature for PMMA

solvt	temp, °C	mass fraction	diffusivity, cm^2 s: this study	diffusivity, cm^2 s: lit.	source
MMA	30	0.09	1.9×10^{-16}	8.0×10^{-14}	Hopfenberg et al.[27]
MeAc	30	0.005	8.5×10^{-13}	5.0×10^{-13}	Wang et al.[28]
MeOH	30	0.005	6.4×10^{-12}	1.6×10^{-11}	Berens et al.[29]

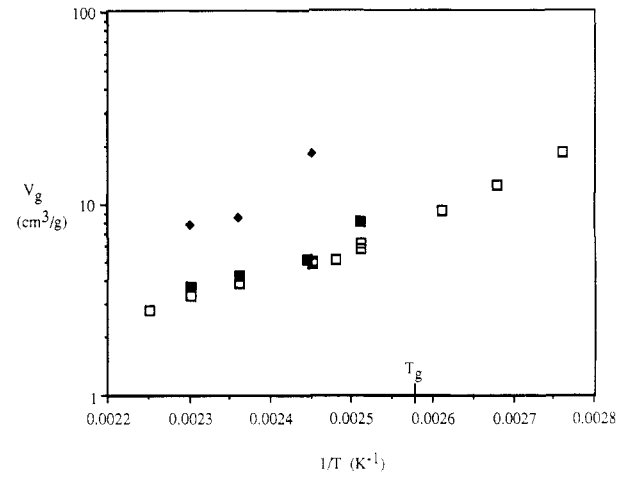

Figure 12. Temperature dependence of the retention volume of solute in PMMA: (□) MeOH; (■) MeAc; (◆) MMA.

Two caveats should be noted concerning any conclusions drawn from these comparisons. Firstly, knowledge of the state of the glass (i.e., the amount of excess free volume frozen in) is essential for any unambiguous comparison of sub-T_g transport measurements; yet, the state of the glass is not known in any of these studies. Secondly, extrapolation of super-T_g diffusivities to sub-T_g temperatures could result in significant uncertainty due to the large curvature in the diffusivity plots near the glass transition temperature. Thus, comparison of IGC results with the vapor sorption results are not expected to yield close agreement.

Retention Volume Measurements. The retention volume, V_g, of MeOH, MMA, and MeAc were measured in this study, and these values are listed in Table V. Plots of log V_g are presented in Figure 12 as a function of the reciprocal temperature. All curves show an upward curvature with decreasing temperature ranging from slight for MeOH to large for MeAc. There is no break or transition in the MeOH retention volume plot in the vicinity of the glass transition, as has been observed when the peak maximum is used as the measure of the retention time. This further supports the use of the mean of the elution curve as the proper measure of the retention time.

Vrentas et al.[30] measured the Flory–Huggins interaction parameter, χ_{12}, of MeOH in PMMA using a vapor sorption technique. Over the temperature range 130–160 °C, they measured an average value of χ_{12} equal to 1.2 ± 0.05. This is consistent with the values of χ_{12} measured in this study, which are listed in Table V.

Reliability of Parameter Estimation. The reliability of the parameter estimation decreases as tailing in the elution curve increases. This is true, regardless of the estimation method used. This is believed to be caused by the loss in precision of the data in the tail of the curve due to its lower signal-to-noise ratio. As tailing increases, the fraction of imprecise data increases and the results become less reliable. Indicators of reliability problems are poor comparison of experimental and theoretical elution curves, loss of reproducibility, and nonconformity to model trends (such as linearity of the plots of the dimensionless second moment versus $1/t_d$).

All of these problems are observed for the MeAc data at 135 °C and for the MMA data at 135.5 and 125.3 °C, where considerable tailing is evident. In fact, only the data taken at the lowest of the three flow rates were acceptable for analysis. The others were rejected due to poor comparison of the experimental and theoretical elution curves, a result of the increased skewing and greater tailing at the higher flow rates. For all elution curves exhibiting significant skewing, the peak maxima of the predicted elution curves consistently exceeded those of the experimental elution curves; the overshoot in the theoretical elution curve of MMA in PMMA at 135.5 °C shown in Figure 8 is typical of highly skewed elution curves. Thus, the precision of the MMA results at 135 °C and MeAc results at 125 and 135 °C is in question.

Modifying the Experiment To Reduce Skewing. The IGC technique is not limited to polymer/solvent systems that exhibit elution curves without significant skewing (a symptom of systems with low diffusivities). All polymer/solvent systems with sufficient solubility can yield elution curves without severe tailing. This can be accomplished by proper modification of the column and film geometries and carrier gas flow rates, as discussed below.

The dimensionless model parameter, β

$$\beta^2 = \frac{\tau^2}{D_p t_d} \tag{46}$$

determines the degree of tailing, where the skewing and length of the tail increases as β^2 increases. Inspection of the variables defining β^2 reveals that tailing increases as the square of the film thickness, τ, increases and decreases with increasing diffusivity, D_p, and carrier gas dead time, t_d. Thus, the increased tailing accompanying solvent/polymer systems with low diffusivities (i.e., as for MMA and MeAc near the T_g) may be compensated for by switching to longer columns with thinner films and by making measurements at smaller carrier gas velocities. In this manner, reliable capillary column IGC results may be obtained for all polymer/solvent systems with sufficient solubility.

Acknowledgment. We thank the National Science Foundation (ENG 79-04168), the Center of the University of Massachusetts/Industry Research on Polymers (CUMIRP), the Rohm and Haas Co., and the University of Massachusetts Computing Center for their support during this research.

Nomenclature

a	parameter characterizing film geometry
b	parameter characterizing film geometry
A_n	coefficient of Fourier expansion of $f(t)$
B_n	coefficient of Fourier expansion of $f(t)$
c	gas-phase solute concentration
c'	stationary-phase solute concentration
$\mathbf{c}$	mean gas-phase solute concentration
c_0	strength of the inlet impulse
De	diffusion Deborah number
D_g	gas-phase diffusion coefficient
D_p	stationary-phase diffusion coefficient
f	arbitrary response curve
f_t	theoretical response curve
f_e	experimental response curve
I	objective function
$I(\omega)$	imaginary part of Fourier transform
K	partition coefficient
L	column length
N	number of discrete points used in numerical Fourier transform
q	dimensionless stationary-phase concentration
Q_i	τ_{min}/τ_{max}
r	radial coordinate
r'	$r - R$
R	radius of the column
$R(\omega)$	real part of Fourier transform
s	Laplace variable
t	time
t_d	residence time of the carrier gas, L/V
T	column temperature
V	mean speed of the carrier gas
V_g	specific retention volume
W	dimensionless film thickness
x	dimensionless axial length
y	dimensionless mobile phase concentration
Y	Laplace transform of exit concentration
z	axial coordinate

Greek Symbols

α	dimensionless solubility parameter
β	dimensionless diffusion parameter
γ	dimensionless axial dispersion parameter
$\Delta\omega$	interval between discrete points, ω_n
$\delta(t)$	Dirac δ function
μ_1	first temporal moment or mean residence time
μ_2^*	second central moment or variance of the concentration distribution
μ_k	kth normalized moment of the elution curve
μ_k^*	kth central moment of the elution curve
η	dimensionless film thickness
θ	dimensionless time
τ	film thickness
τ_m	mean film thickness
τ_{min}	minimum film thickness
τ_{max}	maximum film thickness
ϕ	azimuthal angle
χ_{12}	Flory–Huggins interaction parameter
Ψ	function of s, eq 23
ω	imaginary space coordinate
ω_n	nth discrete point in imaginary space
Ω	interval of integration of Fourier transform

Registry No. MMA, 80-62-6; PMMA, 9011-14-7; MeOH, 67-56-1; benzene, 71-43-2; toluene, 108-88-3; ethylbenzene, 100-41-4; polystyrene, 9003-53-6; methyl acetate, 79-20-9.

References and Notes

(1) Pawlisch, C. A.; Macris, A.; Laurence, R. L. *Macromolecules* **1987**, *20*, 1564.
(2) Braun, J. M.; Guillet, J. E. *Adv. Polym. Sci.* **1976**, *21*, 107.
(3) Gray, D. G. *Prog. Polym. Sci.* **1977**, *5*, 1.
(4) Conder, J. R.; Young, C. L. *Physicochemical Applications of Gas Chromatography*; Wiley: New York, 1979.
(5) Laub, R. J.; Pecsok, R. L. *Physicochemical Applications of Gas Chromatography*; Wiley: New York, 1978.
(6) Tewari, Y. B.; Schreiber, H. B. *Macromolecules* **1972**, *5*, 329.
(7) Tait, P. J. T.; Abushihada, A. M. *J. Chromatogr. Sci.* **1979**, *17*, 219.
(8) Braun, J. M.; Poos, S.; Guillet, J. E. *Polym. Lett.* **1976**, *14*, 257.
(9) Kong, J. M.; Hawkes, S. J. *Macromolecules* **1975**, *8*, 685.
(10) Millen, W.; Hawkes, S. *J. Chromatogr. Sci.* **1977**, *15*, 148.

(11) Galin, M.; Rupprecht, M. C. *Polymer* **1978**, *19*, 506.
(12) Hu, D. S.; Han, C. D.; Stiel, L. I. *J. Appl. Polym. Sci.* **1987**, *33*, 551.
(13) Munk, P.; Card, C. W.; Hattam, P.; El-Hibri, M. J.; Al-Saigh, Z. Y. *Macromolecules* **1987**, *20*, 1278.
(14) Vrentas, J. S.; Duda, J. L. *J. Polym. Sci., Polym. Phys. Ed.* **1977**, *15*, 441.
(15) Pawlisch, C. A. Ph.D. Dissertation, University of Massachusetts at Amherst, 1985.
(16) Ramachandran, P. A.; Smith, J. M. *Ind. Eng. Chem. Fundam.* **1978**, *17*, 148.
(17) Radeke, K. H. *Ind. Eng. Chem. Fundam.* **1981**, *20*, 302.
(18) Haynes, H. W. *Chem. Eng. Sci.* **1975**, *30*, 955.
(19) Boersma-Klein, W.; Moulijn, J. A. *Chem. Eng. Sci.* **1978**, *34*, 959.
(20) Johnson, J. L.; Fan, L. T.; Wu, Y. S. *Ind. Eng. Chem. Process Des. Dev.* **1971**, *10*, 425.
(21) Hays, J. R.; Clements, W. C. Jr.; Harris, T. R. *AIChE J.* **1967**, *13*, 375.
(22) Dahlquist, G.; Bjorck, A. *Numerical Methods*; Prentice Hall: Englewood Cliffs, NJ, 1974.
(23) Weinberger, H. F. *A First Course in Partial Differential Equations*; Wiley: New York, 1965.
(24) Vrentas, J. S.; Duda, J. L. *J. Appl. Polym. Sci.* **1978**, *22*, 2325.
(25) Hu, D. S.; Han, C. D. *J. Appl. Polym. Sci.* **1987**, *34*, 423.
(26) Zhurkov, S. N.; Ryskin, G. V. *Zh. Tekh. Fiz.* **1954**, *24*, 797.
(27) Hopfenberg, H. B.; Stannett, V. T.; Jacques, C. H. M. *J. Appl. Polym. Sci.* **1975**, *19*, 2485.
(28) Wang, T. T.; Kwei, T. K. *Macromolecules* **1973**, *6*, 919.
(29) Berens, A. R.; Hopfenberg, H. B. *J. Membr. Sci.* **1982**, *10*, 283.
(30) Vrentas, J. S.; Duda, J. L.; Hsieh, S. T. *Ind. Eng. Chem. Prod. Res. Dev.* **1983**, *22*, 326.

Anomalous Small-Angle X-ray Scattering from a Sulfonated Polystyrene Ionomer

Y. Samuel Ding,[†,§] Stevan R. Hubbard,[‡,⊥] Keith O. Hodgson,[‡] Richard A. Register,[†] and Stuart L. Cooper*[,†]

Department of Chemical Engineering, University of Wisconsin—Madison, Madison, Wisconsin 53706, and Departments of Chemistry and Applied Physics, Stanford University, Stanford, California 94305. *Received September 1, 1987; Revised Manuscript Received December 2, 1987*

ABSTRACT: Anomalous small-angle X-ray scattering has been employed to study the morphology of a nickel-neutralized sulfonated polystyrene ionomer, with particular emphasis on the characteristic upturn in scattered intensity near zero angle. The results indicate that the zero-order scattering is related to the ionomer's neutralizing cation. Applying the Debye–Bueche random two-phase model to the data indicates that the heterogeneity giving rise to the zero-angle scattering has a much larger length scale and smaller electron density difference than the aggregate–matrix scattering and may be due to an inhomogeneous distribution of isolated ionic groups in the matrix.

I. Introduction

Small-angle X-ray scattering (SAXS) has been shown to be a powerful technique for characterizing the morphology of ionomers,[1-10] but to correlate SAXS results with the physical, chemical, or transport properties, ionomer morphology must be understood. Typical ionomer SAXS patterns contain a peak with a Bragg spacing typically 20–100 Å and a strong upturn in intensity as zero angle is approached. The peak has been taken as a signature of ionic aggregation since it was first observed,[1] and numerous SAXS studies have established the validity of this assignment.[1-10] But while several detailed ionomer morphological models have been proposed,[9,10] none can fit both the peak and the upturn with a consistent set of parameters. As a result, Yarusso and Cooper[10] have suggested that the upturn might be artifactual, possibly arising from residual camera scattering or impurities or voids in the samples. Recent work by Kumar and Pinéri[8] shows that scattering from a uniformly electron dense but finite sample volume gives an upturn qualitatively similar to that observed in ionomers. However, the calculated intensity from this source is considerably smaller than what is observed, meaning that an additional source of scattered intensity must exist.

To determine whether the cations in the ionomer give rise to the observed upturn as well as peak scattering, it would be highly desirable to separate scattering involving the cation from nonionic scattering sources. Selectively changing the scattering power of one of the scattering elements in a material has been widely used for this purpose in mineral and biological crystallography. One often-used method is to prepare a second material which has the same structure as the one under study, but with one type of atom replaced with one much lighter or heavier (known as an isomorphous derivative); however, this procedure suffers from the difficulty of producing two samples of identical morphology.[11] Another means of varying scattering contrast is to perform a set of complementary scattering experiments (X-ray, neutron, electron) on a single sample,[12] but a single sample is generally unsuitable for more than one type of experiment. Recently, with the availability of intense, continuously tunable X-rays from synchrotron sources, anomalous small-angle X-ray scattering (ASAXS) has been demonstrated as a uniquely powerful method for changing the scattering contrast of a selected element.[11,13-19] This paper describes the application of ASAXS to a nickel-neutralized sulfonated polystyrene ionomer.

II. Experimental Section

A. Sample Preparation. The sulfonated polystyrene studied was obtained from Dr. Robert Lundberg and the late Dr. Henry Makowski of the Exxon Research and Engineering Co. and was

* To whom correspondence should be addressed.
† University of Wisconsin—Madison.
‡ Stanford University.
§ Present address: Baxter Healthcare Corporation, Round Lake, IL 60073.
⊥ Present address: Department of Biochemistry and Molecular Biophysics, College of Physicians and Surgeons of Columbia University, New York, NY 10032.

0024-9297/88/2221-1698$01.50/0